Broad-Band Near-Infrared Plasmonic Nanoantennas for Higher Harmonic Generation

Miguel Navarro-Cia* and Stefan A. Maier

Experimental Solid State Group, Department of Physics, Imperial College London, London SW7 2AZ, United Kingdom

ABSTRACT

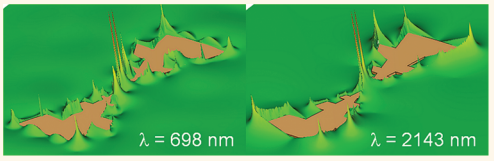

We propose a broad-band near-infrared trapezoidal plasmonic nanoantenna, analyze it numerically using finite integration and difference time domain techniques, and explain qualitatively its performance *via* a multidipolar scenario as well as a conformal transformation. The plasmonic nanoantenna reported here intercepts the incoming light as if it were of cross-sectional area larger than double its actual physical size for a 1500 nm bandwidth expanding from the near-infrared to the visible spectrum. Within this bandwidth, it also confines the incoming light to its center with more than 1 order of magnitude field enhancement. This wide-band operation is achieved due to the overlapping of the different dipole resonances excited across the nanoantenna. We further demonstrate that the broad-band field enhancement leads to efficient third harmonic generation in a simplified wire trapezoidal geometry when a Kerr medium is introduced, due to the lightning rod effect at the fundamental and the Purcell effect at the induced third harmonic.

KEYWORDS: broad-band · conformal transformation · nanoantenna · plasmonic · third harmonic generation

Antennas[1] are widely used at radio and microwave frequencies to couple/radiate energy from a source to free space with a far-field emission of reduced angular divergence. Due to reciprocity, they also collect radiation efficiently from defined directions. These functionalities are performed *via* the manipulation of enhanced fields in subdiffraction volumes. With the advent of nanotechnology, antennas operating at optical/near-infrared frequencies have become accessible,[2] exceeding the energy localization capabilities of traditional optical elements such as mirrors and lenses.[3] Optical antennas[2] can be advantageously used to either harvest or focus light in nanoscale volumes not limited by diffraction. This results in a large electromagnetic field enhancement in the proximity of the antenna. Likewise, they tailor the excitation and emission processes of nearby fluorescent molecules or quantum dots.[4−6] These abilities hold significant promise for optical emitters, photovoltaics, spectroscopy, and nonlinearities.[2,7−12]

Most nanoantennas reported in the literature so far (nanorods and nanodipoles) show a narrow-band response because of their dipolar nature.[1,7] However, it would be highly desirable to have a nanoantenna with significant bandwidth of operation, for example, more than an octave. Nanoantennas with such properties are expected to make significant contributions,[2] for instance, in the burgeoning areas of surface-enhanced linear/nonlinear vibrational spectroscopy[13,14] and spontaneous two-photon emission,[15,16] which are intrinsically multiwavelength and broad-band in nature, and in higher harmonic generation. We will focus on the latter in this article. Indeed, a broad-band plasmonic nanoantenna could be used for more specific applications linked to harmonic generation, such as perfect lensing *via* phase conjugation and time reversal by enhancing the efficiency of nonlinear processes not only at the fundamental[17] but also at the harmonic frequency.

In an effort to surpass the inherently limited narrow-band operation of infrared frequencies, nanorods and the bow-tie topology have been extensively explored. Nevertheless, their bandwidths of operation are significantly below an octave.[11,15,16,18,19] Other attempts less explored involve the use of fractal topologies,[20] multielement arrangements,[21−23] or the interaction with grating modes.[24] However, they also experience limitations. For instance, the fractal Sierpinski nanocarpet[20] has strong field enhancement at several wavelengths, but the spatial position of the hot spot is wavelength-dependent; multi-nanodipoles of different

* Address correspondence to m.navarro@imperial.ac.uk.

Received for review February 7, 2012 and accepted March 19, 2012.

Published online March 19, 2012
10.1021/nn300565x

lengths arranged radially[21,22] require circularly/elliptically polarized light to excite the resonance of each nanodipole, and the bandwidth is constrained to the number of different nanodipoles that one can set radially; like fractal nanoantennas, the hot spot location of an array of nanorods of different length[23] is wavelength-dependent; finally, the grating-assisted multiwavelength nanoantenna[24] requires several gratings of different periodicities, leading to impractical large structures. For microwave frequencies, broad-band antennas (with bandwidths up to 10:1, *i.e.*, decade or even higher) were introduced in the 1950s *via* so-called frequency-independent antennas.[1,25] Similar to the history of the development of optical bow-tie and Yagi-Uda dipolar antennas,[2,7] microwave designs of broad-band antennas are also attractive starting points for broad-band optical nanoantennas. Indeed, one can find a compact advanced design such as the trapezoidal logperiodic antenna,[1,25] which displays a broad-band single hot spot without the need for circularly/elliptically polarized light.

The article is structured as follows: first, the trapezoidal logperiodic nanoantenna is presented and characterized in terms of cross sections and field enhancement at the gap and vertexes. Second, the underlying physics of the nanoantenna is qualitatively described from a simple multidipolar scenario and by a conformal transformation approach. This study will allow us to subsequently propose a simplified design geometry, which would alleviate demands on the manufacturing process while retaining all features associated with the broad-band trapezoidal nanoantenna. Finally, third harmonic generation is demonstrated *via* a Kerr medium placed at the gap between the arms of the simplified nanoantenna. All numerical calculations assume, for simplicity, that the single nanoantenna is surrounded by free space.

RESULTS AND DISCUSSION

Extinction, Scattering, and Absorption Cross Sections. A trapezoidal nanoantenna is displayed in Figure 1a, where the geometrical parameters are defined as follows: $R_{i+1}/R_i = \alpha^{0.5}$ with i = 1, 2...5, R_1 = 1000 nm, and α, which controls the width of the teeth, variable from 0.39 to 0.74 in 0.05 steps; inner and outer angle $\theta_i = 30°$ and $\theta_o = 60°$, respectively; metal thickness t = 60 nm; separation between top and bottom arms g = 50 nm. For the finite integration time domain simulations,[26] the metal is assumed to be silver, with a permittivity following the Drude model $\varepsilon_{Ag} = \varepsilon_0(\varepsilon_\infty - (\omega_p^2/\omega(\omega - i\gamma))$, with ε_∞ = 4.039, plasma frequency $\omega_p = 1.39077 \times 10^{16}$ rad/s, and damping constant $\gamma = 1.23955 \times 10^{15}$ rad/s. Notice that γ has been overestimated compared to Johnson and Christy[27] to account for imperfections in a real situation and to reduce computational time. For accurate calculation of the scattering properties and the field distribution close to the metal, several precautions were taken, which are detailed in Methods.

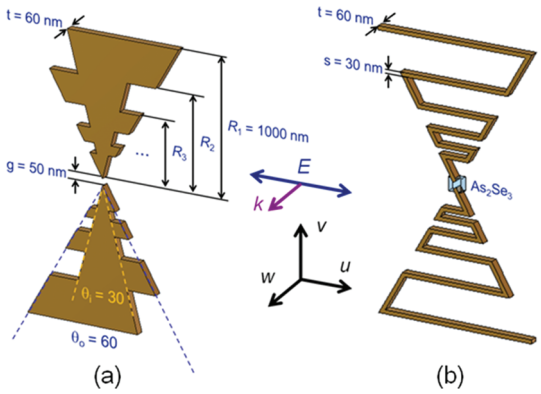

Figure 1. Schematic geometry of the solid (a) and wire (b) trapezoidal nanonantenna. The nanoantennas are illuminated by a *u*-polarized plane-wave propagating in the *w*-direction.

Initially, the dependence of the cross section on the teeth number is investigated for a nanoantenna with α = 0.49, as seen in Figure 2a. As expected from the microwave counterpart of the nanoantenna,[1,25] the inclusion of additional teeth increases the nanoantenna's bandwidth. Thus, this design allows for a systematic widening of the wavelength bandwidth constrained only by space limitations. In Figure 2a, one can identify three peaks in the extinction cross section for a 4-tooth nanoantenna, whereas five peaks emerge for a 6-tooth nanoantenna. This suggests that the number of peaks for the extinction cross section is $N - 1$, where N is the number of teeth. The origin of this relation is elucidated below.

Unlike dipole and bow-tie antennas, the fundamental operation of the trapezoidal tooth nanoantenna is induced by a normal-incident plane-wave polarized *perpendicular* to the axis aligned with the two arms of the nanoantenna.[1,25,28] For more information, the reader is referred to the Supporting Information. On the left-hand side of Figure 2b, the charge density distribution at the plane of the middle cross section of the nanoantenna is plotted for all resonance peaks shown in panel a. In addition, the perspective view of the field enhancement (*i.e.*, $|E|/|E_{incident}|$) at the middle cross section of the nanoantenna is displayed on the right-hand side. An inspection of these charge densities shows that two opposite neighboring teeth of each arm of the nanoantenna are active at each resonance in a dipole fashion. These local dipoles at each arm are in phase with each other and mainly oriented in the *u*-direction. Otherwise, they would not be induced by a *u*-polarized plane-wave. Likewise, the charge densities confirm that a local vertical dipole between arms is induced for each resonance at the center gap. Nevertheless, this dipole is not induced directly by the coupling to the incident field given their cross-polarization

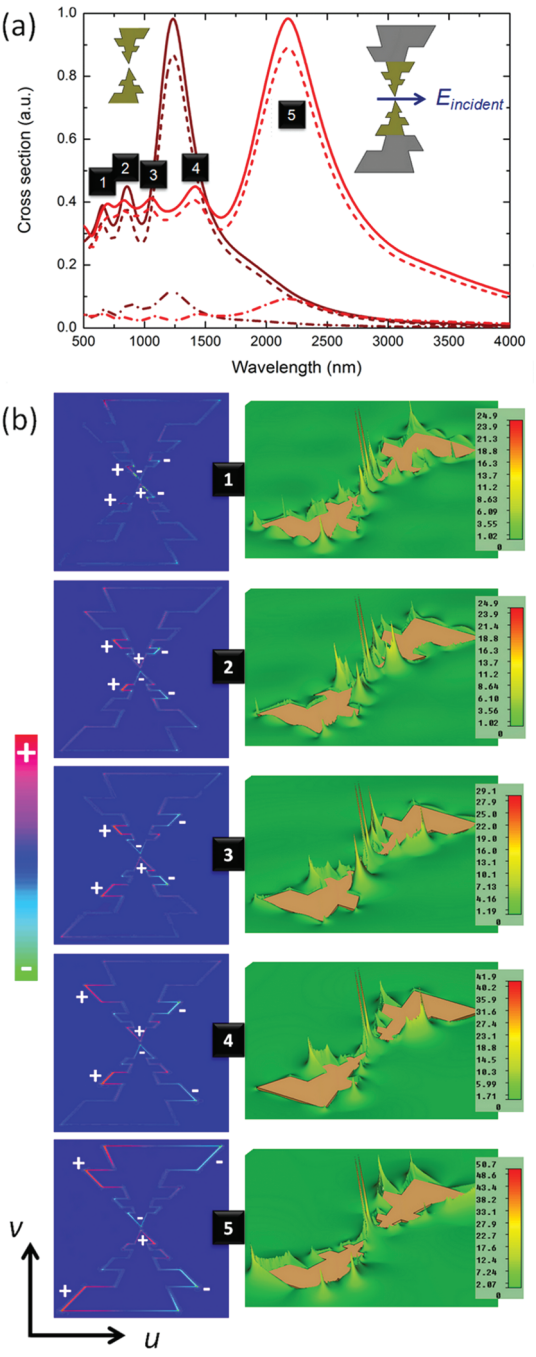

Figure 2. (a) Extinction (solid), scattering (dashed), and absorption cross section (dash-dot) for a 4- (dark red) and 6-tooth trapezoidal nanoantenna (red) with α = 0.49 when the structure is illuminated by a *u*-polarized plane-wave. The numbers account for the peak order. (b) From top to bottom: first, second, third, fourth, and fifth resonance according to panel a. Static charge density at the middle cross section of the nanoantenna (left) and field enhancement at the cross-sectional plane of the nanoantenna (right). The + and − symbols superimposed underline the associated charge distribution. Notice that each field enhancement plot has its own scale bar.

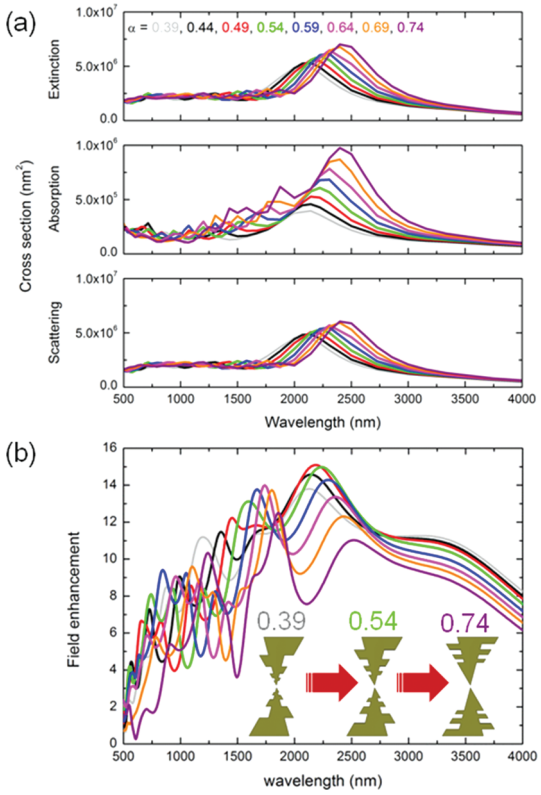

Figure 3. (a) From top to bottom, extinction, absorption, and scattering cross section of a 6-tooth trapezoidal nanonantenna with varying α parameter, *i.e.*, tooth width. Notice the different scale of the absorption cross section. (b) Field enhancement with respect to the incident field, $|E|/|E_{incident}|$, at the center of the nanonantenna as a function of the α parameter.

but by the currents excited in the nanoantenna by the teeth-based dipoles. These charge densities along with the field enhancement put also in evidence that the active region shifts from the ends of the nanoantenna toward its center as the wavelength decreases, leading to larger field localization. Finally, the field enhancements highlight that the gap between arms is indeed a broad-band hot spot since it always shows the largest field enhancement across the nanoantenna for all resonant peaks. Further information about the field distribution and induced current at the middle cross section of the nanoantenna can be found in the Supporting Information. Notice that the absolute value of the field enhancement should be taken with precautions since it depends on the mesh grid, and ideal infinitely small grid mapping perfectly all sharp features would lead to larger field enhancements than those reported here. Nevertheless, in the real experiment, blunt nanoantennas are measured, and thus, the results should be closer to the simulation with a mesh grid like the one used here (mesh cell resolution up to 1 nm × 1 nm × 5 nm in the zone between arms) rather than an ideal infinitely small grid.

From the local dipole picture, we can foresee a red shift of the bandwidth of operation as the parameter α increases (*i.e.*, thinner teeth) because, then, the distance between the charges of different sign in each local dipole are larger. In addition, in general, the larger/longer the physical area/length of the nanoantenna, the larger the scattering.[1] Figure 3a shows clear

evidence of the two trends described above, where the extinction, absorption, and scattering cross sections are plotted for various values of the α parameter at a range of wavelengths.

Currently, nanoantennas can find extremely useful applications by incorporating nonlinear media or immobilizing/retaining a biological recognition element at the spatial location of maximum field enhancement (hot spot).[2,7,8,12−14,17] For that reason, the effect that the parameter α has on the field enhancement (with respect to the incident field) at the center gap of the nanoantenna is shown in Figure 3b. In passing, notice that the largest field enhancement does not happen at the center but at the central vertexes of the arms; see Figure 2b and Figure S3. According to our simulations, the field is expected to be enhanced 15 times at the lowest resonant wavelength and is kept 10 times higher than the incident field for a wide wavelength range for the chosen gap of 50 nm. Although these values do not outperform those of other nanoantennas (*e.g.*, dipole and bow-tie nanoantennas) already reported in the literature, the nanoantenna proposed in this article has the outstanding advantage to maintain large extinction cross sections and high field enhancements at a single position, the center, at a truly broad-band spectrum.

Conformal Transformation Explanation. The broad-band performance of the trapezoidal nanoantenna and a number of its key physical properties can also be understood using coordinate transformation, in a similar fashion to touching plasmonic elements.[29,30] Since the proposed system is admittedly far more complex than previous examples because the quasi-static limit approximation is no longer valid and it is a three-dimensional finite system, the analysis presented below is only qualitative.

Let us consider an infinite two-dimensional system that inherently has a broad-band response: a line dipole aligned along the *y*-axis at $x = -\infty$ between two semi-infinite metal strips lined up along *x*; see Figure 4a. If the strips represent a perfect electric conductor, this configuration is the well-known parallel plate waveguide, which has a broad-band response with two straight lines of slope 45° passing through the origin of the $k_0-\beta$ diagram representing either forward- or backward-traveling waves.[25] Thus, the spectrum is continuous and broad-band. If now corrugations with period *p* are applied to the semi-infinite metal strips, the dispersion relation becomes a typical periodic stop- and pass-band;[25] see Figure 4b.

Let us now apply the following conformal transformation on the above structure:[28,31]

$$z' = e^{z} \qquad (1)$$

where both *z* and *z*′ are complex numbers with the convenient form $z = x + iy$ and $z' = u + iv = \rho e^{i\varphi}$.

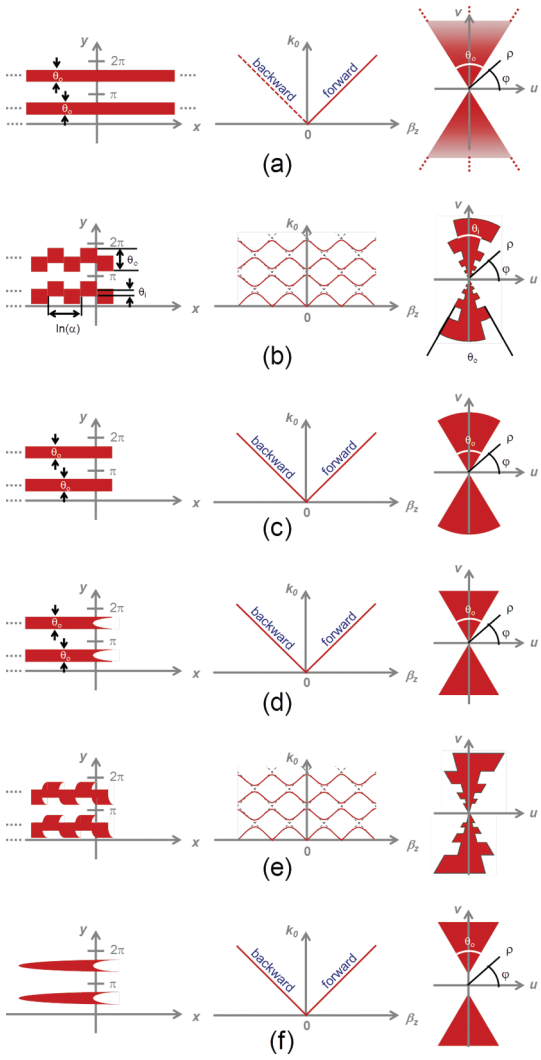

Figure 4. From left to right: two metallic slabs (*z*-plane), dispersion diagram, and transformed structures (*z*′-plane): semi-infinite (a) and truncated slabs (b−f). The dipole source at $x = -\infty$ is transformed into a dipole at the vertex. If the metallic slabs are either infinitely long (a) or are terminated in a matched (nonreflecting) load, only those branches of the dispersion curve which have positive slope are applicable. Hence, the nonexcited backward-traveling mode is displayed as a dashed line in panel a. When a termination is present as it is the case for the rest, the branches with negative slope are also valid.

Obviously, all points at $x = -\infty$ in *z* translate to the origin in *z*′, and vertical and horizontal lines in the *z*-plane are converted to circles and radial lines in the *z*′-plane. Hence, the resulting structure is a smooth and tooth bow-tie for the smooth and corrugated parallel plate waveguide, respectively. Likewise the line dipole source in *z* translates to a point dipole at the origin in *z*′ aligned along the *v*-axis. Hence, if the bow-tie structure of infinite extend is fed at the vertex, it shows a broad-band nature since the original and transformed structure have the same spectral response.[29−31] Indeed, from antenna theory and microwave designs, we know that the bow-tie response is broad-band.[1] Similarly, if the tooth bow-tie is fed at the vertex, its

response is periodic.[1,25,28] Notice that a truncation in z, which means that our parallel plate waveguide does not extend to infinity, leads to a truncation in z'; see Figures 4b–f. However, the broad-band character remains as long as standing waves are not excited. In terms of the z-plane, this can be ensured if the reflected traveling wave is negligible by, for instance, a lossy (*i.e.*, the metal is no longer a perfect electric conductor but has certain, yet high, conductivity) waveguide long enough for the forward-traveling wave to decay before reaching the end or by placing an absorbing material at the end. This undesired backward-traveling mode excitation *via* the finite length of the structure is known as the "end effect" in microwave antenna engineering.[1,25,28] Finally and more interesting is the situation when the arms of the bow-tie do not touch at a single point, but they are moved apart a certain distance, as it is the case in reality; see Figure 4f. This modification maps in the z-plane as an adiabatic truncation of the slabs before reaching $x = -\infty$, and the hypothetical line dipole connecting arms in the z'-plane transforms to a line dipole connected to both strips at the end of them. These alterations are not expected to cause any significant change in the electromagnetic response of the parallel waveguide and, thus, of the bow-tie antenna, either smooth or tooth kind.

For a real metal represented *via* a Drude function, the previous qualitative discussion is completely valid. However, the dispersion diagram for the smooth bow-tie does not extend infinitely following the light line as it would happen in an ideal perfect electric conductor parallel plate waveguide, but it bends over approaching an asymptotic limit corresponding to the surface plasmon frequency.[32] Given that this limit happens at near-infrared, one can still consider the system broad-band (it operates from DC to near-infrared).[29] For the tooth bow-tie, on the contrary, the dispersion relation exhibits qualitatively the same induced periodicity as that of the perfect electric conductor case.

Wire Trapezoidal Nanoantenna: Harmonic Generation with a Nonlinear Kerr Medium. Given the fact that the mechanism of this nanoantenna can be understood as originating from a collection of individual dipole antennas resonating at different wavelengths (Figure 2b and Figure S2), one could suggest replacing the trapezoidal nanoantenna with an array of dipole nanoantennas. This simplification preserves the broad-band scattering characteristics, but at the expense of having several hot spots rather than a single hot spot for the whole frequency bandwidth (see Figure 2b and Supporting Information for more details), which is crucial for the harmonic generation scheme proposed below. Nevertheless, one can envision a similar simplification, which preserves the broad-band scattering as well as single-spot features: the trapezoidal nanoantenna can be transformed to a winding wire nanoantenna; see Figure 1b, with wire width s = 30 nm in the case

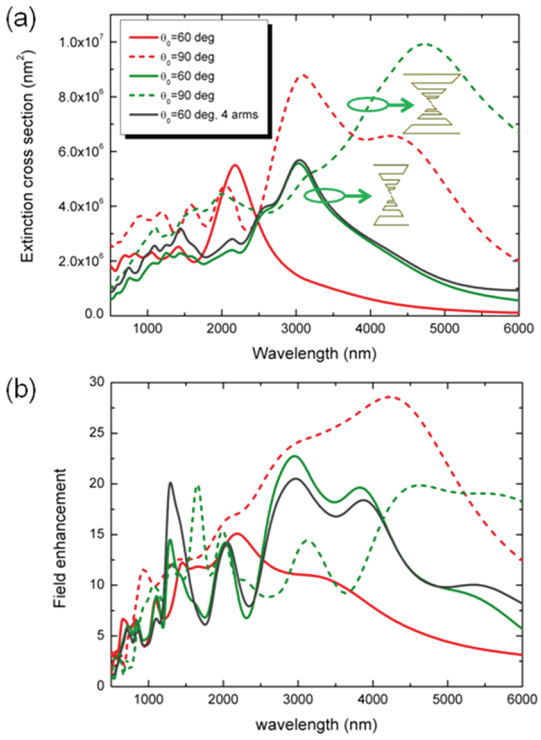

Figure 5. (a) Extinction cross sections of the two-arm solid (red) and wire trapezoidal nanonantenna (dark green) and four-arm wire trapezoidal nanoantenna (dark gray) for θ_0 = 60° (solid) and 90° (dashed) and α = 0.49. (b) Field enhancement with respect to the incident field at the center of the nanonantenna.

discussed here. The extinction cross section and field enhancement at the center are plotted in Figure 5 and compared with the case of a solid trapezoidal antenna with outer angle θ_o = 90°. As it is apparent, the wire antenna performs very closely to the solid one. The two most distinctive consequences of the simplified wire design are as follows: the response experiences a red shift, and additional resonant peaks or shoulders emerge. These features stem from the fact that, now, the nanoantenna can be understood as an array of six horizontal nanorods (connected) inducing at least six resonances rather than five. The upper-most nanorod, which is indeed the extra resonant element compared to the solid trapezoidal nanoatenna, admits an induced dipole with larger distance between charges than anyone excited in the solid trapezoidal nanoantenna. Therefore, it resonates at longer wavelengths.

Finally, we investigate harmonic generation with the wire trapezoidal nanoantenna. Second- and third-order susceptibilities in optical nonlinear media are, in general, several orders of magnitude smaller than the first-order linear susceptibility.[33] It has been shown that nonlinear processes can be enhanced, however, *via* the use of plasmonic nanoantennas, whose collective oscillation of electrons at their surface enhances the local field intensity by several orders of magnitude.[2,7,8,12–16,18,32,34] As a further refinement of this scheme, two independent narrow-band nanoantennas

aligned orthogonally have been recently suggested to be used in second harmonic generation.[35] With this approach, four optimal processes work together to increase the efficiency of the harmonic generation: first, one of the two nanoantennas captures the incident field at the fundamental frequency; second, *via* the so-called lightning rod effect, the local field intensity is greatly enhanced at the gap between arms where the nonlinear medium is smartly placed; third, the nonlinearity generates the corresponding harmonic dipole; fourth, the radiation of this harmonic dipole is increased by the second nanonantenna working specifically at such frequency *via* the Purcell effect.

It can be intuitively understood that a broad-band nanoantenna would be able to enhance the harmonic generation of any order (*i.e.*, second, third, *etc.*) of any fundamental frequency falling within its bandwidth of operation. Furthermore, by employing an additional broad-band nanoantenna orthogonally to the first one, a polarization-independent scheme is easily envisaged. This assumption is confirmed in Figure 5, where a four-arm wire trapezoidal nanoantenna displays almost identical extinction cross section and field enhancement to our two-arm wire trapezoidal nanoantenna regardless of the incident polarization.

To study this proposal, finite difference time domain calculations[36] were performed where the Drude parameters of the silver have been fitted to Johnson and Christy.[27] The Kerr medium is assumed to be chalcogenide glass[33] As_2Se_3 with $n_0 = 2.53$ ($\varepsilon_r = 6.4009$) and $\chi^{(3)} = 6.8 \times 10^{-18}$ m^2/V^2 and fills a volume between arms of 100 nm $\times$ 100 nm $\times$ 60 nm; see Figure 1b. To reduce computing resources, the total-field scattered technique has been used. For more details of the simulations, the reader is referred to Methods at the end of the article.

The extinction cross section for the wire trapezoidal nanoantenna loaded with a linear dielectric with the same relative permittivity as the As_2Se_3 and excited by a narrow temporal pulse with amplitude of 1×10^7 V/m is plotted in Figure 6. This peak amplitude has been chosen to fulfill the condition $\chi^{(3)}|E(t)|^2 \ll \varepsilon_r$; see the field intensity (in logarithm scale) in the inset of Figure 6. The results are in agreement with those previously shown in Figure 5. When the isolated Kerr medium is illuminated by a Gaussian wave packet centered at $\lambda = 3$ μm (the largest resonant wavelength of the loaded nanoantenna according to the previous curve) and spectral width of 0.088 μm, no significant third harmonic generation is observed; see dotted line in Figure 6. However, when the nanoantenna is introduced, for the same long-standing pulse (narrow in frequency), a noticeable signal is radiated by our nanoantenna at the third harmonic. Indeed, the intensity of the third harmonic is 9 orders of magnitude higher than without the nanoantenna. In addition, note the 6 orders of magnitude difference between

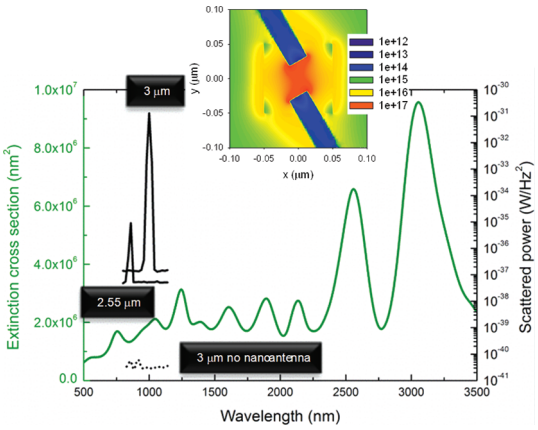

Figure 6. Extinction cross section (dark green) when the nanoantenna is loaded by a linear dielectric with $\varepsilon_r = 6.4009$ and third harmonic radiated power with (solid black) and without nanoantenna (dotted black) for the nonlinear case when the excitation is a quasi-monochromatic plane-wave polarized along *u* with central wavelength of $\lambda = 2.55$ and 3 μm. Top inset: field intensity $|E|^2$ (logarithm scale) at the middle cross section of the loaded nanoantenna for $\lambda = 3$ μm.

the peak intensity and the noise floor. Finally, if the central wavelength of the Gaussian wave packet is changed to 2.55 nm, the intensity of the third harmonic signal is still several orders of magnitude higher than that without a nanoantenna as well as the peak-to-noise ratio, which proves all of our assumptions and shows the potential of introducing broad-band nanoantennas in the field of nonlinearities.

CONCLUSIONS

In conclusion, a broad-band nanoantenna has been shown and analyzed *via* finite integration time domain simulations. For an antenna with a physical cross section of 8.45×10^5 nm^2, the scattering cross section peaks at 7.0×10^6 nm^2 for the longest wavelength resonance and is kept at 2.2×10^6 nm^2 for a 1500 nm bandwidth expanding from the near-infrared to the visible spectrum. Up to 15- and 14-fold field enhancement at the center and up to 50.7 and 41.9 at the vertexes of the plasmonic nanoantenna is obtained at the peak and in the spectrally flat regime, respectively. The underlying physics has been captured in a simple yet powerful way by identifying its multidipolar nature. Also, concomitant with this viewpoint, the conformal transformation has been brought about to shed further light in the mechanism of the nanoantenna. These interpretations have allowed us to simplify the nanostructure without causing any penalty on its response in terms of extinction cross section and field enhancement at the hop spot, that is, the vertex of the nanoantenna. Finally, benefited by the wide-band response of the simplified wire trapezoidal nanoantenna, a compact and flexible third harmonic generation scheme is proposed and validated *via* finite difference time domain simulations. The results shown in this article are a significant step forward toward

wide-band or multiwavelength, flexible, and compact plasmonic devices for general purposes and, in particular, for surface-enhanced spectroscopy and nonlinear processes. The breadth and utility of these applications in biosensing and generating extreme ultraviolet radiation laser pulses suggests that broadband antennas at the nanoscale may play a large role in driving the basic research as well as technology.

METHODS

Finite Integration Time Domain Method: Linear Analysis. Extinction, scattering, and absorption cross sections as well as near-field distribution are calculated using the commercial full-wave three-dimensional software CST Microwave Studio.[26] The dielectric response of silver is modeled as a Drude function of the form $\varepsilon_{Ag} = \varepsilon_0(\varepsilon_\infty - (\omega_p^2/\omega(\omega - i\gamma))$, with $\varepsilon_\infty = 4.039$, plasma frequency $\omega_p = 1.39077 \times 10^{16}$ rad/s, and damping constant $\gamma = 1.23955 \times 10^{15}$ rad/s. For accurate calculation of the scattering properties and the field distribution close to the metal, several precautions are taken. We make sure that the distance between the structure and the perfectly matched layers defining the simulation volume is at least of half wavelength size; subgridding techniques are used to have a mesh cell resolution up to 1 nm × 1 nm × 5 nm in the zone between arms, and the residual energy in the calculation volume is 1×10^{-8} of its peak value. The time stepping stability factor is set to 1, which corresponds to a time step, δt, of around 0.0023 fs. The solver is automatically restarted twice with a reduced time step after an instability abort. The maximum simulation time addressed by the reference excitation signal is set to 45 fs. Therefore, all of our simulations have an excess of around 19 300 time steps. The nanoantenna in a uniform dielectric medium ($n = 1$) is illuminated with a *u*-polarized plane-wave propagating along *w*. The extinction, σ_{ext}, scattering, σ_{scatt}, and absorption cross section, σ_{abs}, are calculated with the solver defined script. To compute the scattering cross section, the radar cross section, that is, the far-field scattered light intensity as a function of angle, is first obtained by integrating the outward power flow over the computational boundaries with an appropriate near- to far-field transform. Then, the scattering cross section, defined as the sum of radar cross section of all angles, is computed. The absorption cross section is obtained by integrating the net power flowing inward over the computational boundaries. Once the scattering and absorption cross sections are known, the extinction cross section is straightforwardly calculated by $\sigma_{ext} = \sigma_{scatt} + \sigma_{abs}$.

Notice that these finite integration time domain simulations have been double-checked with finite difference time domain calculations with similar setup parameters as described below in the nonlinear analysis.

Finite Difference Time Domain Method: Nonlinear Analysis. All spectra and field distributions in the section devoted to harmonic generation are calculated using the commercial software Lumerical FDTD Solutions 7.5.[36] The dielectric response of silver is modeled using a 3 Drude-Lorentzian term fit to the experimentally measured permittivity.[27] We characterize the chalcogenide glass[33] As_2Se_3 with $n_0 = 2.53$ ($\varepsilon_r = 6.4009$) and $\chi^{(3)} = 6.8 \times 10^{-18}$ m^2/V^2 and fills a volume between arms of 100 nm × 100 nm × 60 nm. To reduce computing resources, the total-field scattered technique is used. As for the linear analysis, we make sure that the distance between the structure and the perfectly matched layers defining the simulation volume is at least of half wavelength size. Convergence testing is done by starting the first calculation with a coarse grid and then reducing the grid size in sequential simulations and comparing their results. This iterative process is stopped when the results of the calculation closely match those of the previous one. The final cubic grid is set to 6 nm × 4 nm × 5 nm, except for the As_2Se_3, where 1 nm × 1 nm × 5 nm cubic grid is applied. The time stepping stability factor is set to 0.95. When the gap is filled by a linear dielectric and excited by a narrow temporal pulse, this stability factor corresponds to a time step $\delta t = 0.0022$ fs. When the gap is excited by a long-standing pulse centered at $\lambda = 3$ nm or $\lambda = 2.55$ nm, it leads to $\delta t = 0.0043$ fs. The maximum simulation time is set to 200 and 2000 fs for the narrow temporal and long-standing pulse simulation, respectively. This leads to our simulations having an excess of around 90 000 and 465 000 time steps for the narrow temporal and long-standing pulse simulation, respectively. Additionally, at the end of the simulation, all field components are checked to see if they decay to zero, thus indicating that the simulation has run for a sufficiently long time for the CW information obtained by Fourier transformations to be valid. The residual energy in the calculation volume is 1×10^{-5} of its peak value. The nanoantenna in a uniform dielectric medium ($n = 1$) is illuminated with a *u*-polarized plane-wave propagating along *w*. The scattering cross section is then obtained *via* the integration of the power flowing outward through a box of monitors located outside of the source, that is, in the scattered field region, whereas the absorption cross section is obtained *via* integration of the net power flowing inward through the monitors placed inside of the total field scattered field source box, that is, in the total field region. The extinction cross section is calculated by the sum of the scattering and absorption cross sections.

Conflict of Interest: The authors declare no competing financial interest.

Acknowledgment. The authors thank A. Liu from Lumerical Solutions, Inc. for her technical support regarding the finite difference time domain simulations. Effort sponsored by Leverhulme Trust, the U.S. Army International Technology Centre–Atlantic (USAITC-A) and the Office of Naval Research (ONR and ONR Global).

Supporting Information Available: When the solid logperiodic nanoantenna is energized at the vertex: radiated power as a function of wavelength and radiation patterns for each resonant peak. For the solid logperiodic nanoantenna illuminated by a *u*-polarized plane-wave as the main body of this paper: static charge density, induced current, field distribution, and *vw* view of the total field enhancement at the *uv* middle cross-section plane. This material is available free of charge *via* the Internet at http://pubs.acs.org.

REFERENCES AND NOTES

1. Balanis, C. A. *Antenna Theory: Analysis and Design*; Wiley-Interscience: Hoboken, NJ, 2005.
2. Novotny, L.; van Hulst, N. Antennas for Light. *Nat. Photonics* **2011**, *5*, 83–90.
3. Born, M.; Wolf, E. *Principles of Optics: Electromagnetic Theory of Propagation, Interference and Diffraction of Light*; Cambridge University Press: Cambridge, UK, 1999.
4. Giannini, V.; Fernández-Domínguez, A. I.; Heck, S. C.; Maier, S. A. Plasmonic Nanoantennas: Fundamentals and Their Use in Controlling the Radiative Properties of Nanoemitters. *Chem. Rev.* **2011**, *111*, 3888–3912.
5. Pfeiffer, M.; Lindfors, K.; Wolpert, C.; Atkinson, P.; Benyoucef, M.; Rastelli, A.; Schmidt, O. G.; Giessen, H.; Lippit, M. Enhancing the Optical Excitation Efficiency of a Single Self-Assembled Quantum Dot with a Plasmonic Nanoantenna. *Nano Lett.* **2010**, *10*, 4555–4558.
6. Kim, M. S.; Park, D. H.; Cho, E. H.; Kim, K. H.; Park, Q.-H.; Song, H.; Kim, D.-C.; Kim, J.; Joo, J. Complex Nanoparticle of Light-Emitting MEH-PPV with Au: Enhanced Luminescence. *ACS Nano* **2009**, *6*, 1329–1334.
7. Bharadwaj, P.; Deutsch, B.; Novotny, L. Optical Antennas. *Adv. Opt. Photonics* **2009**, *1*, 438–483.
8. Schuller, J. A.; Barnard, E.; Cai, W.; Jun, Y. C.; White, J.; Brongersma, M. L. Plasmonics for Extreme Light Concentration and Manipulation. *Nat. Mater.* **2010**, *9*, 193–204.

9. Atwater, H. A.; Polman, A. Plasmonics for Improved Photovoltaic Devices. *Nat. Mater.* **2010**, *9*, 205–213.
10. Knight, M. W.; Sobhani, H.; Nordlander, P.; Halas, N. J. Photodetection with Active Optical Antenna. *Science* **2011**, *332*, 702–704.
11. Shegai, T.; Miljković, V. D.; Bao, K.; Xu, H.; Nordlander, P.; Johansson, P.; Käll, M. Unidirectional Broadband Light Emission from Supported Plasmonic Nanowire. *Nano Lett.* **2011**, *11*, 706–711.
12. Liu, N.; Tang, M. L.; Hentschel, M.; Giessen, H.; Alivisatos, A. P. Nanoantenna-Enhanced Gas Sensing in a Single Tailored Nanofocus. *Nat. Mater.* **2011**, *10*, 631–636.
13. Schumacher, T.; Kratzer, K.; Molnar, D.; Hentschel, M.; Giessen, H.; Lippitz, M. Nanoantenna-Enhanced Ultrafast Nonlinear Spectroscopy of a Single Gold Nanoparticle. *Nat. Commun.* **2011**, *2*, 333.
14. Le, F.; Brandl, D. W.; Urzhumov, Y. A.; Wang, H.; Kundu, J.; Halas, N. J.; Aizpurua, J.; Nordlander, P. Metallic Nanoparticle Arrays: A Common Substrate for Both Surface-Enhanced Raman Scattering and Surface-Enhanced Infrared Absorption. *ACS Nano* **2008**, *2*, 707–718.
15. Nevet, A.; Berkovitch, N.; Hayat, A.; Ginzburg, P.; Ginzach, S.; Sorias, O.; Orenstein, M. Plasmonic Nanoantennas for Broad-Band Enhancement of Two-Photon Emission from Semiconductors. *Nano Lett.* **2010**, *10*, 1848–1852.
16. Ko, K. D.; Kumar, A.; Fung, K. H.; Ambekar, R.; Liu, G. L.; Fang, N. X.; Toussaint, K. C., Jr. Nonlinear Optical Response from Arrays of Au Bowtie Nanoantennas. *Nano Lett.* **2011**, *11*, 61–65.
17. Chen, P.-Y.; Alù, A. Subwavelength Imaging Using Phase-Conjugating Nonlinear Nanoantenna Arrays. *Nano Lett.* **2011**, *11*, 5514–5518.
18. Zuloaga, J.; Prodan, E.; Nordlander, P. Quantum Plasmonics: Optical Properties and Tunability of Metallic Nanorods. *ACS Nano* **2010**, *4*, 5269–5276.
19. Fromm, D. P.; Sundaramurthy, A.; Schuck, P. J.; Kino, G.; Moerne, W. E. Gap-Dependent Optical Coupling of Single "Bowtie" Nanoantennas Resonant in the Visible. *Nano Lett.* **2004**, *4*, 957–961.
20. Volpe, G.; Volpe, G; Quidant, R. Fractal Plasmonics: Subdiffraction Focusing and Broadband Spectral Response by a Sierpinski Nanocarpet. *Opt. Express* **2011**, *19*, 3612–3618.
21. Unlü, E. S.; Tok, R. U.; Şendur, K. Broadband Plasmonic Nanoantenna with an Adjustable Spectral Response. *Opt. Express* **2011**, *19*, 1000–1006.
22. Tok, R. U.; Ow-Yang, C.; Şendur, K. Unidirectional Broadband Radiation of Honeycomb Plasmonic Antenna Array with Broken Symmetry. *Opt. Express* **2011**, *19*, 22731–22742.
23. Miroshnichenko, A. E.; Maksymov, I. S.; Davoyan, A. R.; Simovski, C.; Belov, P.; Kivshar, Y. S. An Arrayed Nanoantenna for Broadband Light Emission and Detection. *Phys. Status Solidi RRL* **2011**, *5*, 347–349.
24. Boriskina, S. V.; Dal Negro, L. Multiple-Wavelength Plasmonic Nanoantennas. *Opt. Lett.* **2010**, *35*, 538–540.
25. Collin, R. E.; Zucker, F. J. *Antenna Theory*; McGraw-Hill: New York, 1969.
26. CST Microwave Studio, http://www.cst.com.
27. Johnson, P. B.; Christy, R. W. Optical Constants of the Noble Metals. *Phys. Rev. B* **1972**, *6*, 4370–4379.
28. DuHamel, R. H.; Isbell, D. E. Broadband Logarithmically Periodic Antenna Structures. *IRE Int. Conv. Rec.* **1957**, *5*, 119–128.
29. Aubry, A.; Lei, D.-Y.; Fernández-Domínguez, A. I.; Sonnfraud, Y; Maier, S. A.; Pendry, J. B. Plasmonic Light-Harversting Devices over the Whole Visible Spectrum. *Nano Lett.* **2010**, *10*, 2574–2579.
30. Fernández-Domínguez, A. I.; Maier, S. A.; Pendry, J. B. Collection and Concentration of Light by Touching Spheres: A Transformation Optics Approach. *Phys. Rev. Lett.* **2010**, *105*, 266807.
31. Luo, Yu; Pendry, J. B.; Aubry, A. Surface Plasmons and Singularities. *Nano Lett.* **2010**, *10*, 4186–4191.
32. Maier, S. A. *Plasmonics: Fundamentals and Applications*; Springer: New York, 2007.
33. Zakery, A.; Elliott, S. R. *Optical Nonlinearities in Chalcogenide Glasses and Their Applications*; Springer: Berlin, 2007.
34. Kim, S.; Jin, J.; Kim, Y.-J.; Park, I.-Y.; Kim, Y.; Kim, S. W. High-Harmonic Generation by Resonant Plasmon Field Enhancement. *Nature* **2008**, *453*, 757–760.
35. Chettiar, U. K.; Engheta, N. Pairs of Optical Nanoantennas for Enhancing Second-Harmonic Generation. In *Frontiers in Optics*, OSA Technical Digest CD; Optical Society of America, 2010; paper FThR5.
36. Lumerical http://www.lumerical.com.